Development of highly efficient sulfur-doped TiO2 photocatalysts hybridized with graphitic carbon nitride

Development of highly efficient sulfur-doped TiO_2 photocatalysts hybridized with graphitic carbon nitride

Kentaro Kondo [a], Naoya Murakami [a], Chen Ye [a], Toshiki Tsubota [a], Teruhisa Ohno [a, b, c] *

[a] Department of Applied Chemistry, Faculty of Engineering, Kyushu Institute of Technology, 1-1 Sensuicho, Tobata, Kitakyushu 804-8550, Japan

[b] JST, PRESTO, 4-1-8 Honcho Kawaguchi, Saitama 332-0012, Japan

[c] JST, ACT-C, 4-1-8 Honcho Kawaguchi, Saitama 332-0012, Japan

Keyword: Graphitic carbon nitride, Sulfur-doped TiO_2, Hybrid semiconductor, Visible-light responsive photocatalyst, Z-scheme reaction

Abstract

Graphitic carbon nitride (g-C_3N_4) has attracted much attention as a metal-free semiconductor having visible light absorption and relatively high chemical stability. In the present study, we hybridized g-C_3N_4 with sulfur-doped TiO_2, which is a visible light-responsive photocatalyst with high oxidation ability, in order to improve photocatalytic activity under visible-light irradiation. Hybrid photocatalysts were prepared by three methods: agate mortar, sonication, and planetary mill. Activities of the hybrid photocatalysts depended on the mixing method. The sample prepared by a planetary mill showed the highest photocatalytic activity, 4-times higher than that of sulfur-doped TiO_2. We concluded that the high activity of the hybridized sample under visible-light irradiation is induced by charge transfer between the two photocatalysts mimicking the Z-scheme in photosynthesis.

1 Introduction

Clean technology utilizing the sunlight and artificial light around us has been attracting much attention in recent years due to concerns about environmental issues, and it has been expanding rapidly worldwide.

Photocatalysts have been studied as a means to utilize the abundant light. Titanium(IV) oxide (TiO_2) has been one of the most attractive materials as a photocatalyst owing to its nontoxicity, availability, superior redox ability, and photostability [1]. However, TiO_2 has a bandgap of 3.0 - 3.2 eV, and ultraviolet (UV) light is vital to its photocatalytic reaction. Therefore, many attempts have been made to design highly active TiO_2 under visible light excitation for utilization of sunlight and indoor light illumination. The most widely used method for this has been impurity doping in TiO_2 since the report by Asahi et al. of anionic nitrogen-doped TiO_2 having photoabsorption and photocatalytic activity under visible-light irradiation [2]. However, visible-light activity of doped TiO_2 has been still low compared to the activity of TiO_2 under UV light irradiation. One possible reason for the low l activity is increase in recombination centers and trapping sites produced by impurity doping.

Here, we focused on a hybrid of two semiconductors to improve photocatalytic activity under visible light irradiation. Some studies using a charge separation model [3-6] or Z-scheme model [7-9] have suggested that charge transfer proceeds at the interface between two semiconductors in a hybrid photocatalyst, resulting in increase in photocatalytic activity. In the case of doped TiO_2, a combination pair that acts as reduction part of the semiconductor with high reductive potential in the Z-scheme model is ideal because most of the doped TiO_2 has difficulty in reduction reaction rather than oxidation reaction.

Recently, graphitic carbon nitride (g-C_3N_4), which is an organic semiconductor with visible-light absorption and high reduction ability, has attracted much attention since it can produce hydrogen from water under visible-light irradiation in the presence of a sacrificial donor [10]. The Bandgap and flat-band potential of g-C_3N_4 were reported to be 2.67 eV and -1.42 V (versus Ag/AgCl, pH 6.6) from estimation by $(\alpha h\nu)^2$ versus photon-energy plots and Mott-Schottky plots, respectively [11]. Thus, g-C_3N_4 has superior reduction ability due to the high potential of the conduction band, though its oxidation ability is inferior. Moreover, g-C_3N_4 can be synthesized by a simple and low-cost route, and it has relatively good stability under light irradiation in a water solution as well as in acid or base solutions due to the strong covalent bonds between carbon and nitride atoms [12].

In this study, we hybridized g-C_3N_4 with cationic sulfur-doped TiO_2 (S-TiO_2). S-TiO_2 has been shown to exhibit visible-light absorption, which is attributed to the formation of an electron-occupied level above the valence band consisting of S 3s states, and to exhibit photocatalytic activity under visible light with

wavelengths up to 550 nm [13]. Recently, there have been several reports on hybrids of g-C_3N_4 with TiO_2 [14], TaON [15], and poly(3-hexylthiophene) [16]. However, a charge separation mechanism was employed in these photocatalysts, and explanation of the mechanism was not sufficient. In the present study, we also elucidated the reaction mechanism of the hybrid photocatalyst by using PL measurement.

2 Experimental Section

2.1. Materials

g-C_3N_4 powders were prepared by heat treatment of melamine (Wako Pure Chemical Industries, Ltd., 99%). Thirty grams of melamine in an alumina pot was heated at 550 ^oC for 4 h with a temperature rise rate of ca. 9 $^oC\ min^{-1}$ in a muffle furnace. S-TiO_2 powders were commercial samples (Toho Titanium Co. Ltd., GPP8Y01) containing 0.04 wt% sulfur. The crystal structure of S-TiO_2 powder was anatase without any other crystal phase. Commercially available anatase TiO_2 (Ishihara Sangyo Co. LTD., ST-21) was used as a reference.

2.2. Preparation of hybrid photocatalysts

S-TiO_2 and g-C_3N_4 were hybridized in the ratio of 2 : 1 (wt : wt) by three methods, i. e., agate mortar method, sonication method and planetary mill method. For the agate mortar method, two kinds of powder were ground by an agate mortar for ca. 15 min. For the sonication method, two kinds of powder were suspended in 20 ml of ion-exchanged water by sonication for 30 min followed by stirring for 3 h. Then the sample was separated by filtration, washed with water several times, and dried in a vacuum drying oven at 60 ^oC overnight. For the planetary mill method, 1.5 g of two kinds of powder and 20 ml of ion-exchanged water were added to a 50 mL agate bowl containing 50 g of yttrium-stabilized zirconia grinding beads (NIKKATO Co. Ltd., Φ = 0.6 mm). Then the agate bowl was put on planetary mill (Fritsch Japan Co. Ltd., Planetary Micro Mill pulverisette 7) and the planetary mill was operated at 750 rpm for 10 min. After removing the beads by screening, the sample was separated by filtration, washed with water several times, and dried in a vacuum drying oven at 60 ^oC overnight. Samples names and the hybrid methods are summarized in Table 1.

2.3. Characterization of prepared samples

Crystal structures of the particles were confirmed by using an X-ray diffractometer (Rigaku, MiniFlex II) with Cu Kα radiation (λ = 1.5405 Å). Functional group vibrations were confirmed by using a Fourier transform infrared spectrometer (JASCO, 4200ST) with a diffuse reflectance accessory (JASCO, DR-81). Diffuse reflectance spectra were measured using a UV-visible spectrophotometer (Shimadzu, UV-2600) equipped with an integrating sphere unit (ISR-2600). The specific surface area (S_{BET}) of the particles was measured by nitrogen adsorption on the basis of the Brunauer–Emmett–Teller equation with a surface area analyzer (Quantachrome, Nova 4200e). The morphology of prepared particles was observed by a scanning electron microscope (SEM; JEOL, JSM-6701FONO). Fluorescence spectra were obtained using a photoluminescence (PL) spectrometer (HITACHI, F-2500).

2.4. Photocatalytic activities

Photocatalytic activities of samples were evaluated by photocatalytic decomposition of acetaldehyde. Two hundred milligrams of powder, which has complete extinction of incident radiation, was spread on a glass dish, and the glass dish was placed in a 125 cm^3 Tedlar bag (Polyvinyl fluoride, AS ONE Co. Ltd.), and then the Tedlar bag was sealed by laminating. Five hundred parts per million by volume of gaseous acetaldehyde was injected into the Tedlar bag, and photoirradiation was performed at room temperature after the acetaldehyde had reached an adsorption equilibrium (after 2 h). In order to estimate dark adsorption ability of the photocatalysts, concentration of acetaldehyde under the absorption equilibrium in the dark was measured. The gaseous composition in the Tedlar bag was 79% N_2, 21% O_2, <0.1 ppmv of CO_2 and 500 ppmv of acetaldehyde, and relative humidity was ca. 30%. A 500-W xenon lamp (Ushio, SX-UI501XQ) was used as a light source and the wavelength of photoirradiation was controlled by L-42 filters (λ > ca. 400 nm, Asahi Techno Glass Co.) with an intensity of 12 mW cm^{-2} being used as the light source. For measurement of action spectra, light-emitting diodes (Nichia NCCU033B, Epitex L415-66-60, Epitex L435-30M32L, Lumileds LXHL-LR3C, Lumileds LXHL-LB3C, Lumileds LHHL-NE98 and Lumileds LXHL-MM1D), which emitted light at wavelengths of ca. 365 nm, 415 nm, 435 nm, 455 nm, 470 nm, 505 nm and 530 nm, respectively, were used. The concentrations of acetaldehyde and carbon dioxide (CO_2) were estimated by gas chromatography (Agilent Technologies, 3000A Micro GC, TCD detector) with OV1 and PLOT-Q columns. The apparent

quantum efficiency (QE) was defined by the following equation because of the 5-hole process for CO_2 production.

3 Results and Discussion

3.1. Characterization

XRD patterns of the prepared g-C_3N_4 showed the strongest peak at 27.4^o, which is attributed to stacking of aromatic systems for graphitic materials, and a weak peak at 13.0^o (data not shown). In FTIR spectra of the prepared g-C_3N_4, characteristic stretching vibration of aromatic CN heterocycles in the region of 1200 to 1700 cm^{-1} and breathing mode of the triazine units in the region of 810 to 900 cm^{-1} were observed (data no shown). These results are similar to results of previously studies [13, 17]. Therefore, it is thought that g-C_3N_4 was obtained from the heat treatment of melamine.

Figure 1 shows diffuse reflectance spectra of prepared samples. S-TiO_2 and g-C_3N_4 exhibited visible-light absorption, and their absorption edges were around 510 nm and 650 nm, respectively. The absorption spectrum of p-g-C_3N_4 was blue-shifted in comparison with that of g-C_3N_4. Ming et al. reported that the absorption spectrum of g-C_3N_4 was blue-shifted by ball mill treatment due to a decrease in particle size [18]. Similarly, in the case of p-g-C_3N_4, planetary mill treatment induced a decrease in particle size of g-C_3N_4, resulting in a blue shift of the absorption spectrum. On the other hand, the absorption spectrum of S-TiO_2 was not changed by planetary mill treatment (data not shown).

Figure 2 shows SEM the micrographs of morphologies of hybrid photocatalysts. S-TiO_2 showed aggregated particles with particle size of several tens of nanometers (Fig. 2a), while g-C_3N_4 showed plate-like particles (Fig. 2b). By treatment with the planetary mill, g-C_3N_4 plate-like particles were pulverized into small particles (Fig. 2c). This agreed with two-fold increase in S_{BET} (Table 1). On the other hand, the morphology (data not shown) and S_{BET} of S-TiO2 particles were not changed by planetary mill treatment (Table 1). In the sample prepared by the agate mortar and sonication method (a-SC and s-SC), two obviously different morphologies

of particles were observed, and agglomerated S-TiO_2 particles were attached on plate-like g-C_3N_4 (Fig. 2d, e). In contrast, there was almost no difference in the morphologies of S-TiO_2 and g-C_3N_4 in the sample prepared by planetary mill method (p-SC) and it seemed that dispersed S-TiO_2 was covered on g-C_3N_4 particles (Fig. 2f). This indicates that g-C_3N_4 was pulverized into smaller particle even in the presence of S-TiO_2 and that dispersed S-TiO_2 particles attached to pulverized g-C_3N_4 particles before being aggregated. Very strong mechanical energy produced by a large amount of beads rotated at high speed may cause a chemical reaction on the surfaces of S-TiO_2 and g-C_3N_4 particles.

3.2. Photocatalytic activity

Figure 3 shows time courses of CO_2 evolution for acetaldehyde decomposition over the prepared samples under visible-light irradiation. All of the hybrid photocatalysts showed higher activity than those of original S-TiO_2 and g-C_3N_4. This synergistic effect between S-TiO_2 and g-C_3N_4 implies that the mechanism mentioned in the introduction proceeded over the hybrid photocatalysts. The p-SC sample showed the highest activity, 4-times higher than those of the original samples in comparison of CO_2 evolution after 24 h of photoirradiation. Although p-SC showed the smallest visible-light absorption among the hybrid photocatalysts with different mixing methods (Fig. 1c-e), it showed the highest activity.

One plausible reason for this is the large S_{BET} of p-SC compared to those of samples prepared by other methods. Actually, g-C_3N_4 after planetary mill treatment (p-g-C_3N_4) showed a higher activity than that of original g-C_3N_4 because of an increase in S_{BET}. However, the sample prepared from p-g-C_3N_4 and S-TiO_2 with an agate mortar (a-SpC) showed a much lower photocatalytic activity than that of p-SC (Table 1). Therefore, the large S_{BET} attributed to pulverization of g-C_3N_4 was not main reason for the high activity of p-SC. Another plausible reason is a large number of contact points between the two semiconductors as observed in SEM images of p-SC (Fig. 2f), compared to those for a-SC and s-SC (Fig. 2d, e). Thus, a large number of contact points induced smooth interfacial charge transfer of electrons and positive holes, resulting in separation of electron-hole pairs. A detailed discussion of the mechanism is given in the following section.

Photocatalytic activities of samples prepared by the three mixing methods in another mixing ratio of S-TiO_2 to g-C_3N_4 were also evaluated. As a result, samples hybridized in the ratio of S-TiO_2 : g-C_3N_4 = 2 : 1 showed the

highest activities, and we considered this ratio to be the optimum mixing ratio for S-TiO_2 and g-C_3N_4.

3.3. PL measurements

In order to confirm that the synergistic effect is due to charge transfer between the two semiconductors, PL measurements were carried out. It has been reported that g-C_3N_4 emits strong PL around 460 nm and that its spectrum depends on the degree of condensation and packing between the layers [19, 20]. Actually, a PL spectrum with a peak wavelength of ca. 460 nm was observed under a excitation wavelength at 330 nm, and it was attributed to bandgap emission, judging from the optical bandgap of 2.7 eV evaluated by a diffuse reflectance spectrum (Fig. 1g). Similarly, strong PL emission of p-g-C_3N_4 was observed, but the PL spectrum with a peak wavelength of ca. 450 nm was blue-shifted by 10 nm from that of pure g-C_3N_4 [18].This was due to a blue shift of absorption spectra of g-C_3N_4 as a result of decrease in particle size induced by planetary mill treatment (Fig. 1f, g). Although S-TiO_2 emits weak PL around 450 nm, its intensity was less than 5% of p-g-C_3N_4. Therefore, PL spectra of the hybridized samples were mainly determined by radiative recombination of electron-hole pairs in g-C_3N_4.

Figure 4 shows PL spectra of p-TC and p-SC under excitation wavelengths at (a) 350 nm and (b) 420 nm. The peak wavelength in PL spectra of p-TC and p-SC was 450 nm, which corresponded to that of p-g-C_3N_4. p-SC showed the same PL spectrum as that of p-TC under excitation at the wavelength of 350 nm (Fig. 4a), while the PL peak intensity of p-SC was smaller than that of p-TC under excitation at the wavelength of 420 nm (Fig. 4b). However, an appreciable difference in morphology of these samples was not observed. Thus, these results suggest that visible light absorption of S-TiO_2 decreased PL peak intensity because ST-21 does not have absorption in the visible-light region (Fig. 1a, b). This decrease in PL peak intensity is presumably due to charge transfer, the mechanism of which strongly depends on whether ST-21 or S-TiO_2 can absorb excitation light. For example, in the case of the p-TC, plausible charge transfer under visible-light irradiation is only electron injection from the conduction band of g-C_3N_4 to the conduction band of TiO_2, resulting in improvement of charge separation. However, photocatalytic activity of p-TC was lower than that of p-g-C_3N_4.This result suggests that electron injection from g-C_3N_4 to TiO_2 does not proceed over p-TC (Fig. 5a). In contrast, a Z-scheme reaction also possibly proceeds over p-SC (Fig. 5b) in addition to the above charge

separation. The smaller PL peak intensity of p-SC than that of p-TC and the lower photocatalytic activity of p-TC indicate that Z-scheme model was main charge transfer path over p-SC rather than the charge separation model. As a result, p-SC can possess both ability for oxidation of S-TiO_2 and ability for reduction of g-C_3N_4. p-SC showed smallest R_{PL} among the prepared samples, and correlation between R_{PL} and photocatalytic activity was found (Table 1). This indicates that photocatalytic activity strongly depended on Z-scheme charge transfer and that a large number of contact points are important for efficient charge transfer.

3.4. Action spectra analysis

Action spectra analysis is useful for understanding a photocatalytic mechanism, especially when using a hybrid photocatalyst prepared from two kinds of semiconductors. Figure 6 shows action spectra for the decomposition of acetaldehyde using p-g-C_3N_4, p-S-TiO_2, p-SC and p-TC. Although the hybrid photocatalysts showed lower apparent QE at excitation of 365 nm, p-SC showed higher apparent QE in the visible-light irradiation, compared to only p-S-TiO_2. Moreover, onset wavelength of the action spectrum of p-SC agreed with the absorption edge of S-TiO_2 (ca. 505 nm), indicating that photoexcitation of both semiconductors was required for a high photocatalytic activity in the visible-light region. This result confirms that Z-scheme reaction proceeds over p-SC because the photoresponses for a Z-scheme phototcatalyst were dominated by absorption of the semiconductor having a wider bandgap [21].

3.5. Stability test

g-C_3N_4 included in the hybrid photocatalysts may be decomposed by photogenerated holes in the hybrid photocatalysts because nonoxide-type photocatalysts are less stable than metal-oxides photocatalysts [22, 23]. In order to ensure stability of the hybrid photocatalyst, recycling reactions for the decomposition of acetaldehyde using p-SC were carried out. Figure 7 shows time courses of CO_2 evolution for acetaldehyde decomposition using p-SC for 300 min of visible-light irradiation. After three recycling reactions, severe reduction of photocatalytic activity was not observed. Therefore, it was found that degradation in performance of p-SC was very small and that a high activity was maintained after several photocatalytic reactions.

4. Conclusions

A highly active photocatalyst under visible-light irradiation for organic decomposition was prepared by hybridization with g-C_3N_4 and S-TiO_2 using a planetary mill. Planetary mill treatment could increase S_{BET} and the number of contact points for charge transfer between the two semiconductors. PL measurements and action spectra analysis revealed that Z-scheme charge transfer occurred over p-SC under visible-light irradiation and that p-SC can utilize both its ability for high oxidation of S-TiO_2 and its ability for reduction of g-C_3N_4.

References

[1] A. Fujishima, T. N. Rao, D. A. Tryk, Journal of Photochemistry and Photobiology C 79 (2000) 1-21.

[2] R. Asahi, T. Morikawa, T. Ohwaki, K. Aoki, Y. Taga, Science 293 (2001) 269-271.

[3] N. Serpone, P. Maruthamuthu, P. Pichat, E. Pelizzetti, H. Hidaka, Journal of Photochemistry and Photobiology A: Chemistry 85 (1995) 247-255.

[4] T. Tatsuma, S. Saitoh, P. Ngaotrakanwiwat, Y. Ohko, A. Fujishima, Langmuir 18 (2002) 7777-7779.

[5] Y. Takahashi, T. Tatsuma, Langmuir 21 (2005) 12357-12361.

[6] Y. Bessekhouad, D. Robert, J. V. Weber Catalysis Today 101 (2005) 315-321.

[7] T. Arai, M. Yanagida, Y. Iwasaki, H. Sugihara, K. Sayama, The Journal of Physical Chemistry C 111 (2007) 7574-7577.

[8] Z. Liu, Z. Zhao, M. Miyauchi, The Journal of Physical Chemistry C 113 (2009) 17132-17137.

[9] X. Wang, G. Liu, Z. Chen, F. Li, L. Wang, G. Q. Lu, H. Cheng, Chemical Communications 23 (2009) 3452-3454.

[10] K. Maeda, X. Wang, Y. Nishihara, D. Lu, M. Antonietti, K. Domen, The Journal of Physical Chemistry C 113 (2009) 4940-4947.

[11] J. Zhang, X. Chen, K. Takanabe, K. Maeda, K. Domen, J. D. Epping, X. Fu, M. Antonietti, X. Wang, Angewandte Chemie International Edition 49 (2010) 441-444.

[12] S. C. Yan, Z. S. Li, Z. G. Zou, Langmuir 25 (2009) 10397-10401.

[13] T. Ohno, M. Akiyoshi, T. Umebayashi, K. Asai, T. Mitsui, M. Matsumura, Applied Catalysis A: General 265

(2004) 115-121.

[14] D. Mitoraj, H. Kisch, Chemistry - A European Journal 16 (2010) 261-269.

[15] S. C. Yan, S. V. Lv, Z. S. Li, Z. G. Zou, Dalton Transactions 39 (2010) 1488-1491.

[16] H. Yan, Y. Huang, Chemical Communications 47 (2011) 4168-4170.

[17] C. Li, X. Yang, B. Yang, Y. Yan, Y. Qian, Materials Chemistry and Physics, 103 (2007) 427-432.

[18] Y. Ming, F. Jianqing, H. Qiao, Journal of Wuhan University of Technology-Mater. Sci. Ed. 25 (2010) 914-918.

[19] A. Thomas, A. Fischer, F. Goettmann, M. Antonietti, J. O. Müller, R. Schlöglb, J. M. Carlsson, Journal of Materials Chemistry 18 (2008) 4893-4908.

[20] D. L. Yu, J. L. He, Z. Y. Liu, B. Xu, D. C. Li, Y. J. Tian, Journal of Materials Science 43 (2008) 689-695.

[21] Y. Sasaki, H. Nemoto, K. Saito, A. Kudo, The Journal of Physical Chemistry C 113 (2009) 17536-17542.

[22] D. Meissner, R. Memming, The Journal of Physical Chemistry 92 (1988) 3476-3483.

[23] J. Aldana, Y. A. Wang, X. Peng, Journal of the American Chemical Society 123 (2001) 8844-8850.

Acknowledgment

This work was supported by the JST PRESTO program and the JST ACT-C program.

Table 1 S_{BET}, R_{PL} and photocatalytic activity of the prepared samples. R_{PL} is intensity ratio of the PL peak attributed to radiative recombination of p-g-C_3N_4 under excitation at the wavelength of 350 to that of 420 nm.

name	sample	treatment	S_{BET} / m^2 g^{-1}	R_{PL}	CO_2 evolution for 24 h / ppmv
TiO_2	TiO_2	no treatment	62	-	21
S-TiO_2	S-TiO_2	no treatment	60	-	150
p-S-TiO_2	S-TiO_2	planetary mill	59	-	278
g-C_3N_4	g-C_3N_4	no treatment	10	-	67
p-g-C_3N_4	g-C_3N_4	planetary mill	21	0.76	257
a-SC	S-TiO_2, g-C_3N_4	agate mortar	43	-	240
s-SC	S-TiO_2, g-C_3N_4	sonication	45	-	163
p-SC	S-TiO_2, g-C_3N_4	planetary mill	63	0.70	708
p-TC	TiO_2, g-C_3N_4	planetary mill	48	0.77	182
a-SpC	S-TiO_2, p-g-C_3N_4	agate mortar	55	0.84	162

Figure 1 Diffuse reflectance spectra of (a) TiO_2, (b) S-TiO_2, (c) p-SC, (d) a-SC, (e) s-SC, (f) p-g-C_3N_4 and (g) g-C_3N_4

Figure 2 SEM images of (a) S-TiO_2, (b) g-C_3N_4, (c) p-g-C_3N_4, (d) a-SC, (e) s-SC and (f) p-SC

Figure 3 Time courses of CO_2 evolution from acetaldehyde decomposition over (a) p-SC, (b) a-SCr (c) s-SC, (d) S-TiO_2 and (e) g-C_3N_4 under visible-light irradiation

Figure 4 PL spectra of p-TC and p-SC under excitation wavelength at (a) 350 nm, (b) 420 nm

Figure 5 Schematic images of photocatalytic reaction and PL emission of (a) p-TC and (b) p-SC under visible-light irradiation.

Figure 6 Action spectra for the decomposition of acetaldehyde using (a) p-S-TiO_2, (b) p-TC, (c) p-SC and (d) p-g-C_3N_4

Figure 7 Recycling reactions for photocatalytic decomposition of acetaldehyde using p-SC

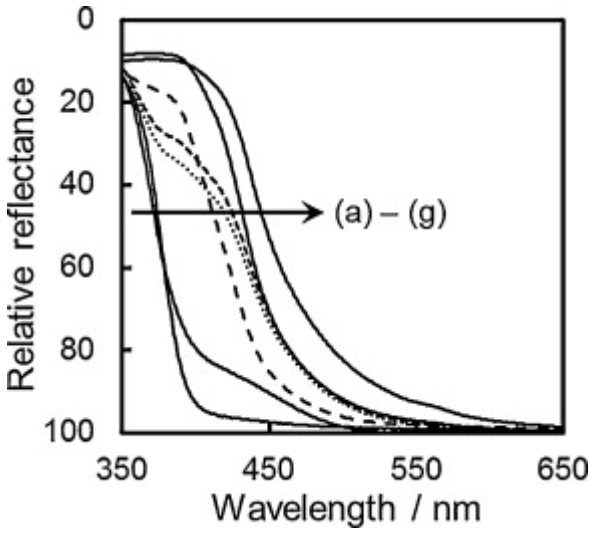

Figure 1 Diffuse reflectance spectra of (a) TiO2, (b) S-TiO2, (c) p-SC, (d) a-SC, (e) s-SC, (f) p-g-C3N4 and (g) g-C3N4

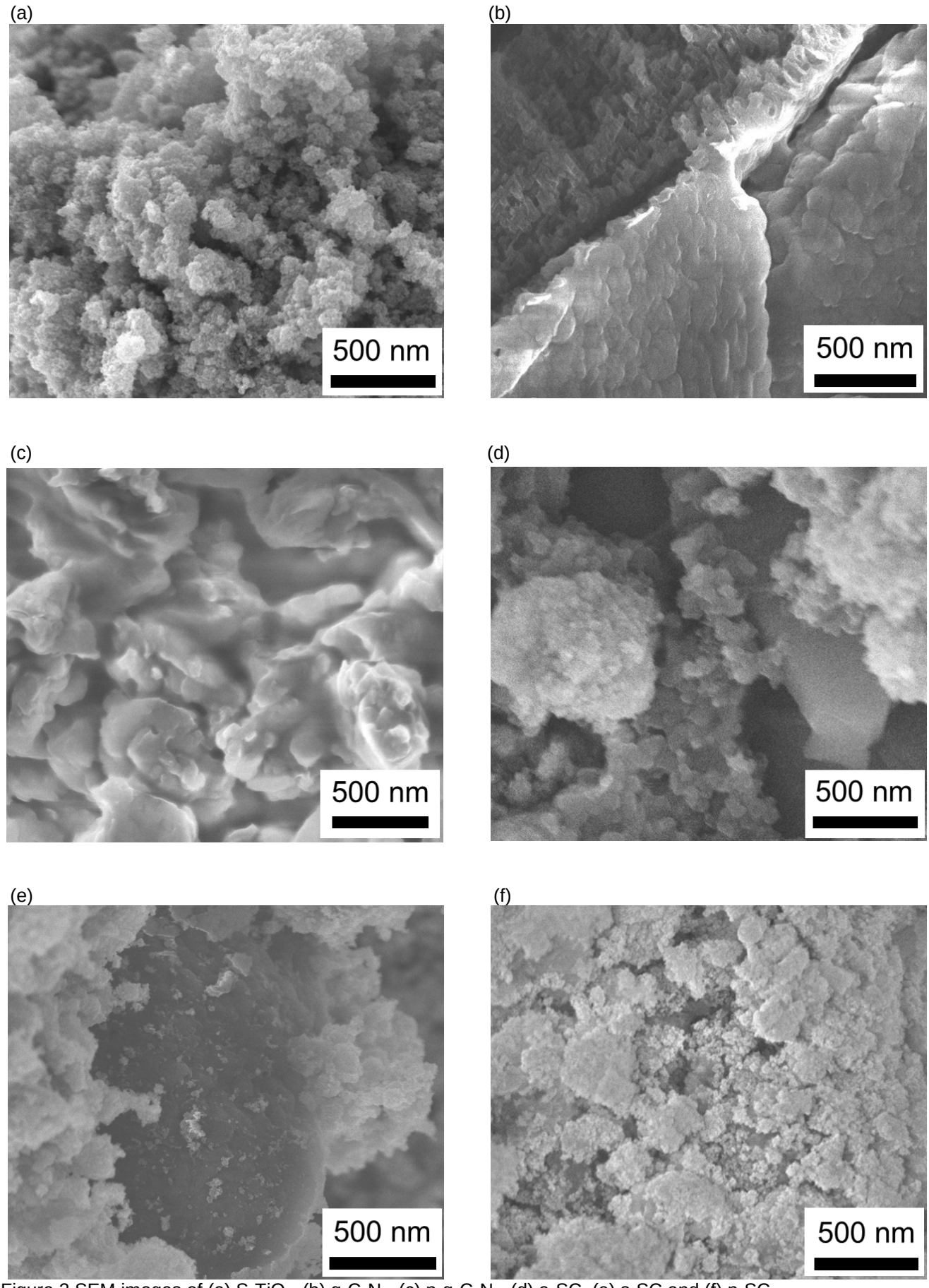

Figure 2 SEM images of (a) S-TiO_2, (b) g-C_3N_4, (c) p-g-C_3N_4, (d) a-SC, (e) s-SC and (f) p-SC

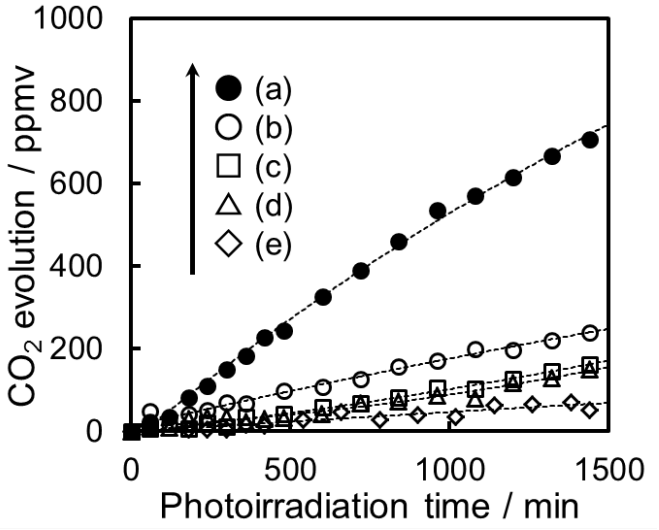

Figure 3 Time courses of CO_2 evolution from acetaldehyde decomposition over (a) p-SC, (b) a-SCr (c) s-SC, (d) S-TiO_2 and (e) g-C_3N_4 under visible-light irradiation

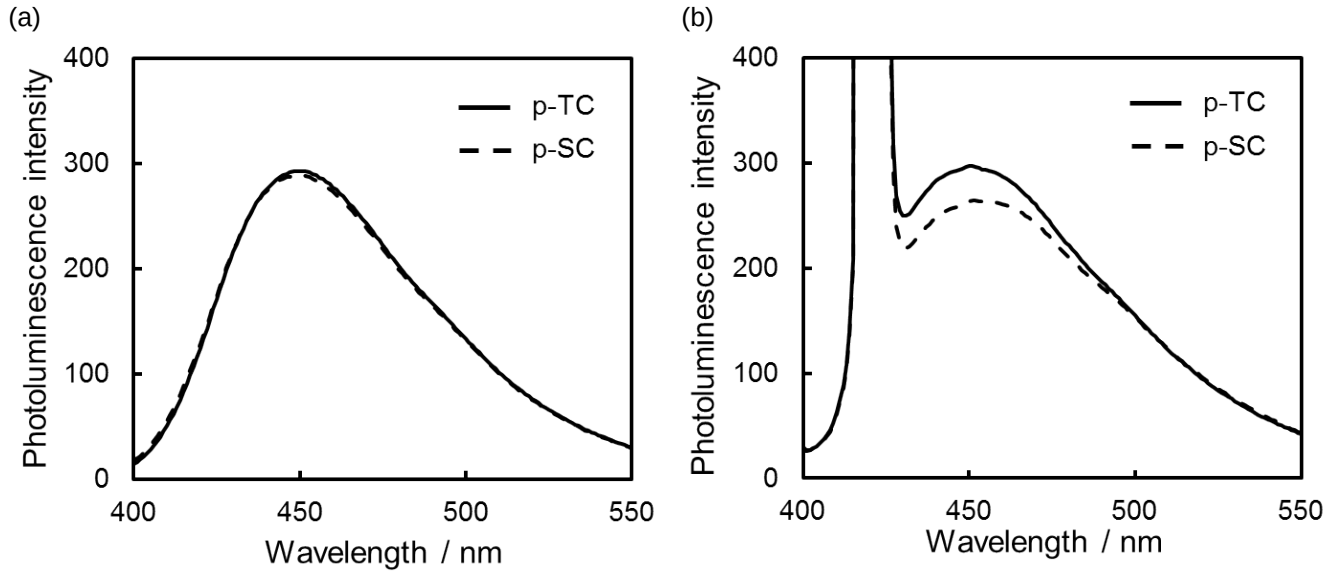

Figure 4 PL spectra of p-TC and p-SC under excitation wavelength at (a) 350 nm, (b) 420 nm

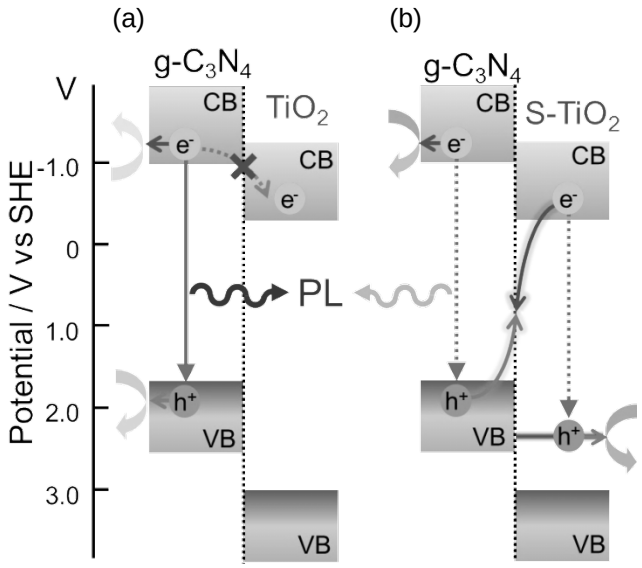

Figure 5 Schematic images of photocatalytic reaction and PL emission of (a) p-TC and (b) p-SC under visible-light irradiation.

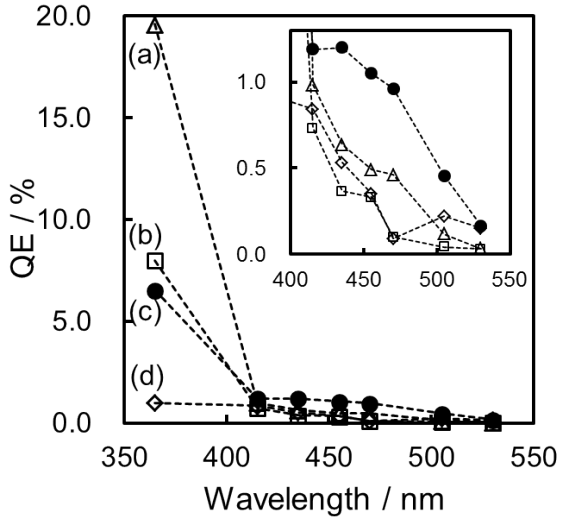

Figure 6 Action spectra for the decomposition of acetaldehyde using (a) p-SC, (b) p-TC, (c) p-SC and (d) p-g-C_3N_4

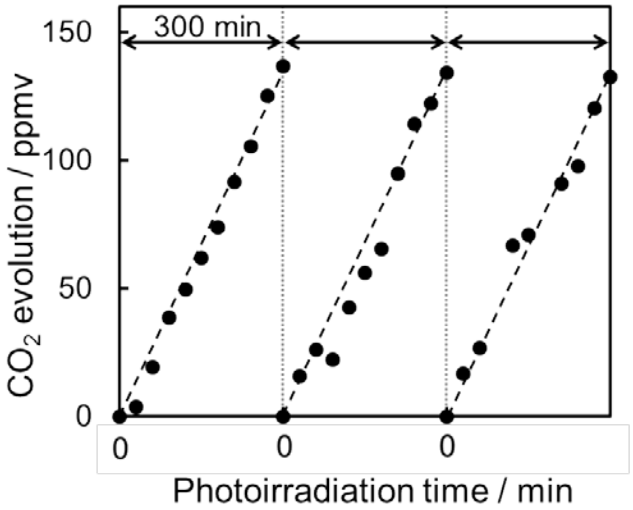

Figure 7 Recycling reaction for photocatalytic decomposition of acetaldehyde using p-SC

Graphical abstract.tif

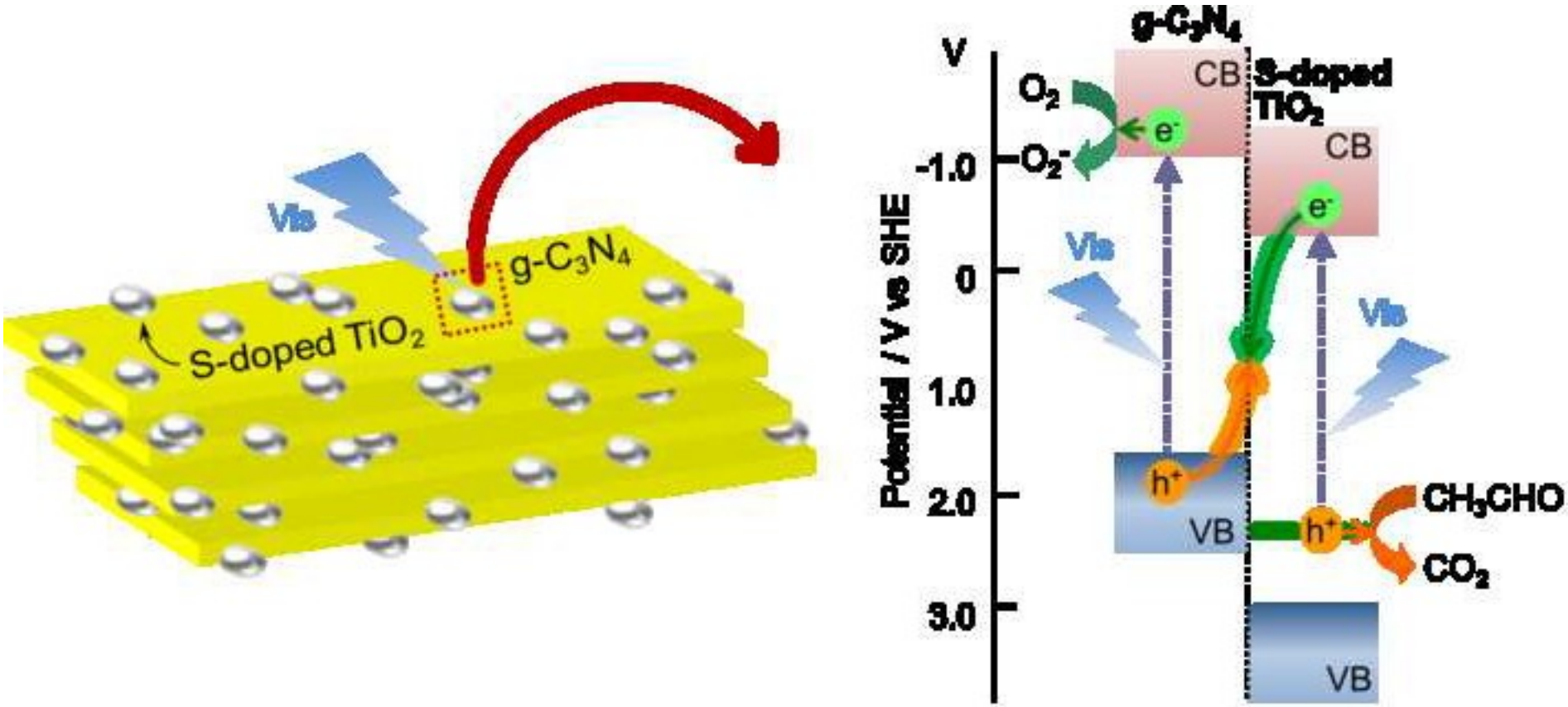

Highlight

Two kinds of powdery semiconductors, S-doped TiO_2 and graphitic carbon nitride, were hybridized.

Photocatalytic activity was evaluated by decomposition of acetaldehyde under visible light.

The activity of the sample prepared by a planetary mill was 4-times higher than that of S-doped TiO_2.

The sample prepared by a planetary mill showed Z-scheme charge transfer under visible light.